Materials Today Communications 39 (2024) 109339

Contents lists available at ScienceDirect

Materials Today Communications

journal homepage: www.elsevier.com/locate/mtcomm

Effect of thermal treatments on the surface electrical conductivity of AlSi7Mg produced by laser powder bed fusion

Silvia Marola [a,b,*], Oscar Antonio Peverini [c], Mauro Lumia [c], Giuseppe Addamo [c], Flaviana Calignano [d], Diego Manfredi [b,e]

[a] Department of Mechanical Engineering, Politecnico di Milano, Via G. La Masa 1, Milano 20156, Italy
[b] Center for Sustainable Future Technologies (CSFT@PoliTo), Istituto Italiano di Tecnologia (IIT), Via Livorno 60, Torino 10144, Italy
[c] Istituto di Elettronica e di Ingegneria dell'Informazione e delle Telecomunicazioni (IEIIT), Consiglio Nazionale delle Ricerche (CNR), Corso Duca degli Abruzzi, 24, Torino 10129, Italy
[d] Department of Management and Production Engineering (DIGEP) – Integrated Additive Manufacturing Center (IAM) - Politecnico di Torino, Corso Duca Degli Abruzzi, 24, Torino 10129, Italy
[e] Department of Applied Science and Technology (DISAT) - Integrated Additive Manufacturing Center (IAM) - Politecnico di Torino, Corso Duca Degli Abruzzi, 24, Torino 10129, Italy

ARTICLE INFO

Keywords:
Laser powder bed fusion
Al-Si alloys
Electrical conductivity
Thermal treatment

ABSTRACT

In the last years, the production of hypoeutectic Al-Si waveguide components by metal additive manufacturing has gained increasing attention in the telecommunications industry. The performances of waveguide components are influenced primarily by dimensional tolerances, surface electrical conductivity, surface roughness, and dimensional accuracy. Among these properties, electrical conductivity is known to be strongly influenced by the structural and microstructural characteristics of the alloys.

In this work, microstructural and structural properties of an hypoeutectic Al-Si alloy, namely the AlSi7Mg alloy, were studied using FESEM, DSC, and XRD to understand how different thermal treatments (stress relieving, T5, and T6) affect the surface electrical conductivity. In the end, the most suitable thermal treatment to be applied to this alloy to maximize its electrical conductivity and, therefore, its appeal for microwave waveguide components is identified.

1. Introduction

Waveguide components are widely used in microwave and millimeter-wave antenna-feed chains developed for different applications, including satellite communications, navigation, and earth observation [1]. In the last years, the production of waveguide components using metal Additive Manufacturing (AM) has been thoroughly investigated [2]. In particular, due to their good electrical and thermal conductivity, hypoeutectic Al-Si alloys, broadly and successfully processed by Laser Powder Bed Fusion (PBF-LB/M), are recognized as a suitable material for the production of waveguide components of industrial interest [3].

One of the key features determining the suitability of a metallic material to produce these components is surface electrical conductivity. It is well known in the scientific literature that electrical conductivity is strongly affected by the structural and microstructural characteristics of the alloys. In particular, crystalline lattice distortion, supersaturation, and sizeable secondary phases can ruin the electrical conductivity making necessary a change in microstructure to improve this property [4–6]. This holds especially in the case of secondary phases having considerably higher resistivity than the matrix, as in Al-Si hypoeutectic alloys. The higher resistivity of the Si phase, 11 orders of magnitude higher than that of α-Al, hinders the electronic transport in the alloy through scattering phenomena that reduce the mean free path of electrons [4,7].

On the other hand, the extremely high and localized heating and cooling rates involved in the PBF-LB/M process promote a microstructural refinement consisting in the transition from plate-like to fibrous Si eutectic and an extension of Si solid solubility [8,9]. Even though the modification of the eutectic morphology has been demonstrated favorable in terms of electrical conductivity, the increased supersaturation along with the lattice distortion generated upon the PBF-LB/M process

* Corresponding author at: Department of Mechanical Engineering, Politecnico di Milano, Via G. La Masa 1, Milano 20156, Italy.
E-mail address: silvia.marola@polimi.it (S. Marola).

https://doi.org/10.1016/j.mtcomm.2024.109339
Received 25 January 2024; Received in revised form 30 April 2024; Accepted 23 May 2024
Available online 24 May 2024

hurt the electrical conductivity of the hypoeutectic Al-Si alloys. An easy and efficient way to recover electrical conductivity is to apply a thermal treatment to the components allowing for the precipitation of solutes, a relaxation of the crystalline lattice, and a modification of the microstructural features, i.e. spheroidization and growth of eutectic Si and precipitates [10].

In this work, microstructural and structural properties of an hypoeutectic Al-Si alloy, namely the AlSi7Mg alloy, were studied using Field Emission Scanning Electron Microscopy (FESEM), Differential Scanning Calorimetry (DSC) and X-Ray Diffraction (XRD) to understand how different thermal treatments, Stress Relieving (SR), T5, and T6, affect the surface electrical conductivity. In the end, the most suitable thermal treatment to be applied to this alloy to maximize its electrical conductivity and, therefore, its appeal for microwave waveguide components is identified.

2. Materials and methods

AlSi7Mg samples, as 10x10x10 mm^3 cubes and test cavities in WR75 and WR28 waveguides (Fig. 1), were produced by Beam-IT SpA using an SLM®280^{HL} machine by SLM Solutions. The powders employed for the PBF-LB/M were provided by Zare srl (Italy) and are characterized by the chemical composition reported in Table 1, by a spherical shape and by a particle size distribution with a d_{10}, a d_{50}, and a d_{90} of 28 μm, 43 μm, and 64 μm respectively. The parameters employed for the sample production are the following: laser power 350 W, scan speed 1150 mm/s, hatch distance 0.17 mm, and layer thickness 50 μm.

The samples were subjected to shot blasting using a Nordblast SD9 machine using a combination of glass and zirconia microspheres with a diameter in the range 63 – 150 μm as reported by Calignano et al. in a previous study [11]. The shot blasting is a simple and fast finishing process used to remove residual sintered particles attached to the component surface and to reduce surface roughness. Then all the samples were subjected to three different thermal treatments: the SR (artificial aging at 300 °C for 2h), the Beam-IT proprietary T5 (artificial aging at low temperature), and T6 (solubilization at 510 °C for 2h + water quench + artificial aging at 160 °C for 8h) treatments. The results obtained from the heat-treated samples were compared with those of an untreated one, indicated as-built (AB) from hereafter. Fig. 2 reports a schematic representation of the thermal treatments performed on the samples.

Table 1
Chemical composition of the AlSi7Mg0.6 powders provided by Zare.

	Al	Si	Mg	Ti	Fe	Zn	Mn	Cu
wt %	Bal.	6.5 – 7.5	0.5 – 0.7	0.1 – 0.18	≤ 0.15	≤ 0.07	≤ 0.05	≤ 0.02

Cubic samples were employed to evaluate the microstructural features and the structural and thermal characteristics, while the test cavities were employed to determine the equivalent surface electrical resistivity upon thermal treatment.

Microstructural analyses were carried out on polished samples etched using a dilute Keller solution using a ZEISS SUPRA TM 40 FESEM. Image analysis for the determination of the perimeter and cross-sectional area of the secondary phases was carried out on at least 5 micrographs using the software Image J. XRD was performed in Bragg-Brentano geometry with a PANalytical X'Pert PRO diffractometer by Philips using the K_α emission line of a Cu filament. Patterns were acquired in the 2θ range from 20° to 140° at steps of 0.013°. The face-centered cubic (fcc) Al lattice parameter was computed with the

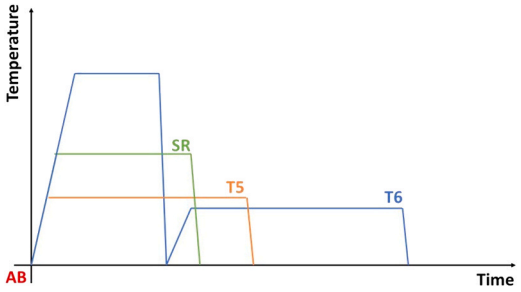

Fig. 2. Schematic representation of the different thermal treatments investigated in this work.

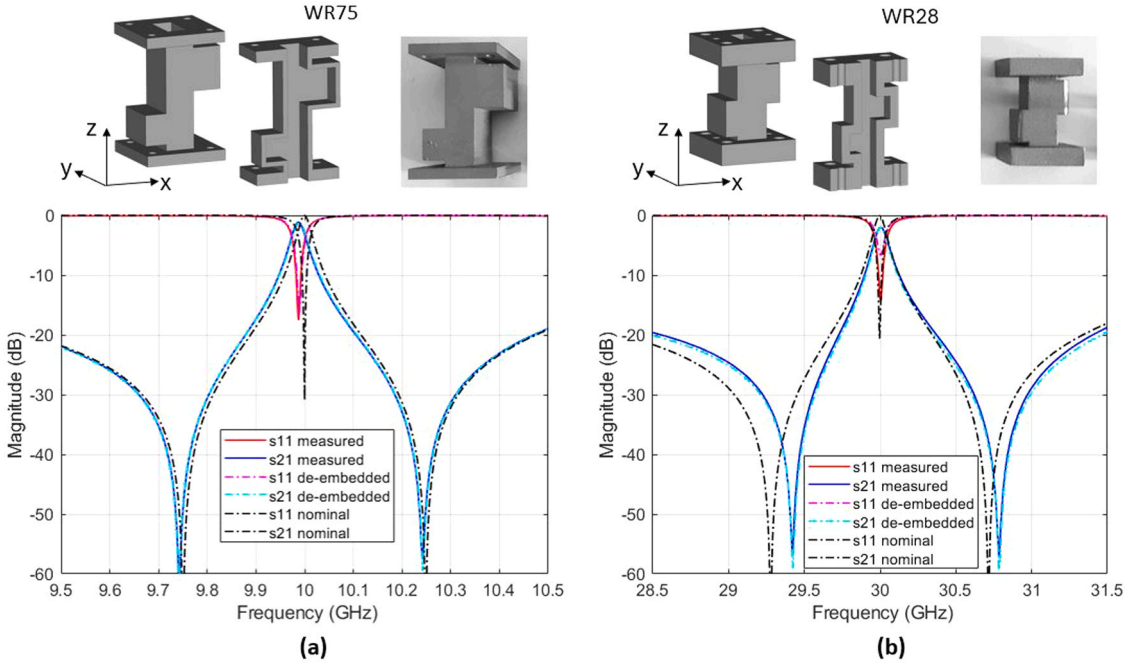

Fig. 1. WR75 (a) and WR28 (b) test cavities. Photos, CAD, and corresponding measured, de-embedded and nominal radio-frequency performance (S11: reflection coefficients; S21: transmission coefficient).

cosθcotθ method to evaluate the degree of Si supersaturation upon heat treatment. Thermal analyses were made under N_2 atmosphere using a NETZSCH DSC 214 Polyma in the temperature range from 50 to 450 °C at the heating rate of 20 °C/min, equilibrating the heat flux at both temperatures.

The electrical surface resistivity was determined by measuring the scattering reflection (S11) and transmission (S21) parameters of the WR75 and WR28 test cavities (Fig. 1) through a vector network analyzer calibrated at the input waveguide ports via the thru-reflection-line technique. Subsequently, a best-fitting procedure has been applied, by which the filter geometry has been varied up to fit the radio-frequency measurements.

Vickers microhardness measurements were performed on samples polished up to 1 μm, through a Future Tech FM-810 Micro Vickers hardness tester by applying a load of 500 gf and a dwell time of 15 s. A mean HV value was derived from at least five measurements.

3. Results and discussion

At first glance, it is possible to see that all the thermal treatments performed on the AlSi7Mg samples strongly affect the microstructural features of this alloy, Fig. 3. In particular, upon every temper, the morphology of the eutectic Si and the amount of Si solubilized in the Al matrix are changed in the alloy. As already well known from the literature [8], the sample in the AB state display a microstructure made of a fibrous Si eutectic forming an almost continuous network around the α-Al cells of few microns in size (Fig. 3a). In some cases, nanometric Si precipitates can be observed inside the Al cells (red arrows in Fig. 3a), indicating Si supersaturation due to the high cooling rates involved in the process. When the AlSi7Mg alloy is subjected to artificial aging at low temperature (T5 temper), the microstructure begins to change, and it is possible to observe abundant precipitation of Si nanocrystals inside the Al cells and a fragmentation of the eutectic Si (Fig. 3c). The presence of precipitation confirms the high supersaturation level of the AB sample. After the T5 thermal treatment, it is still possible to recognize the peculiar microstructure characteristic of the Al-Si alloys processed by PBF-LB/M, but there is a reduction of Si supersaturation possibly promoting relaxation of the crystalline lattice. Increasing the artificial aging temperature to 300 °C (SR treatment), it is possible to observe a further change in the microstructure. After this temper, Si appears spheroidized and almost homogeneously dispersed inside the Al matrix (Fig. 3b). Due to the abundant eutectic fragmentation and the coalescence of the nanometric precipitates, Si always appears to be sub-micrometric in size. Moreover, the cellular microstructure observed for the AB and T5 is almost entirely lost. When the AlSi7Mg samples are subjected to a solubilization treatment at high temperature followed by quench and artificial aging at low temperature (T6 temper), the microstructural features totally change. As visible from Fig. 3d, after this temper, the microstructure is made of an Al matrix containing large Si platelets, homogeneously dispersed throughout the sample. The features deriving from the PBF-LB/M process are entirely lost upon this temper.

From the micrographs reported in Fig. 3, it appears that the thermal treatments have a strong effect on the Si morphology in the different AlSi7Mg samples. Considering these morphological changes is of particular interest because it is reported in the literature that the cross-section dimension of the secondary phase, Si in this specific case, is strictly related to the electrical resistivity of the alloys due to a change in the mean free path of electrons caused by scattering phenomena at the interface between matrix and secondary phases. In particular, the resistivity (ρ) is reported to increase when the P/S ratio increases, in which P and S represent the perimeter and the cross-sectional area of the secondary phase, respectively [7,12,13]. The graph in Fig. 3e represents the trend of the P/S ratios for the AlSi7Mg samples subjected to the different thermal treatments considered here. The results reported in that graph suggest that the samples subjected to the SR and T5 tempers possess a better electrical conductivity than the others, possibly thanks to the presence of more rounded Si cross-sections and the reduced distortion of the crystalline lattice.

Further analyses were performed using DCS and XRD (Fig. 4) to verify if the thermal treatments used in this work can promote Si precipitation and lattice relaxation. In particular, the DSC was employed to investigate the temperature range from 100 to 400 °C, in which the precipitation of secondary phases occurs (Fig. 4a). What was observed is that, in the AB sample, there are two exothermic signals associated with Si and minority compound precipitation [8], while in the heat-treated samples precipitation has already occurred. In particular, the sample subjected to the T6 temper displays a broader precipitation signal centered at approximately 300 °C suggesting that Si is partially precipitated after this heat treatment, but some elements (e.g. Mg) are still in solution in the α-Al matrix. On the contrary, samples subjected to the T5 and SR tempers do not display any precipitation signals, indicating that the supersaturated elements were rejected from the Al crystalline lattice.

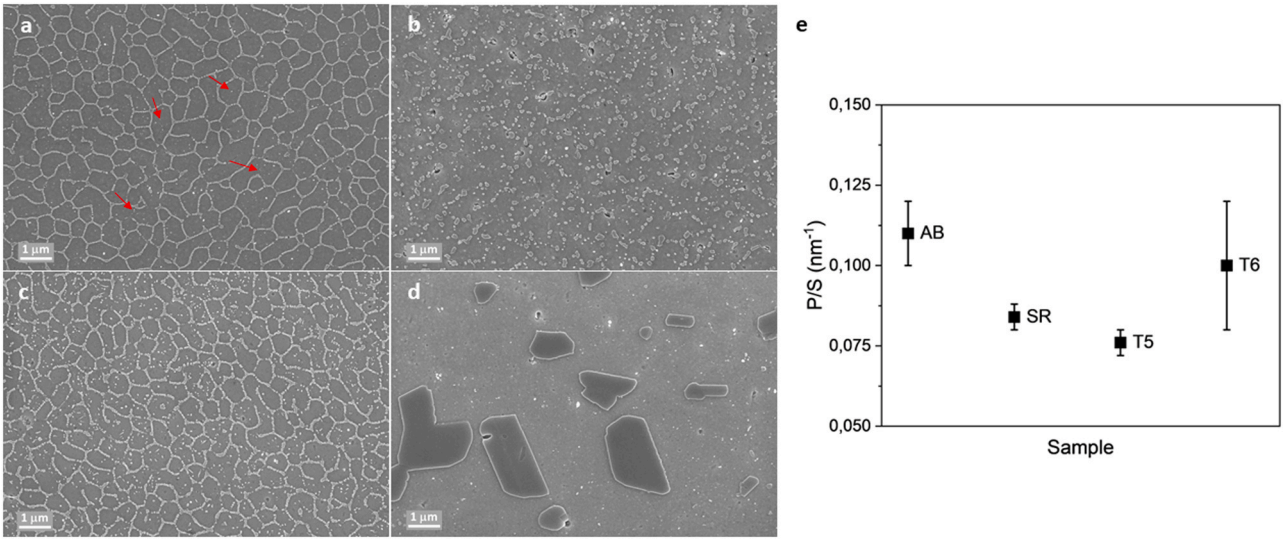

Fig. 3. Micrographs of the AlSi7Mg alloy subjected to different tempers (a-d) and trend of the perimeter over area ratio of the Si crystals (e). In particular (a) represent the microstructure in the as built state, (b) the one after the stress relieving treatment, (c) that related to the T5 temper and (d) that associated with the T6 thermal treatment. The red arrows in (a) point at the nanometric Si precipitates inside the α-Al cells.

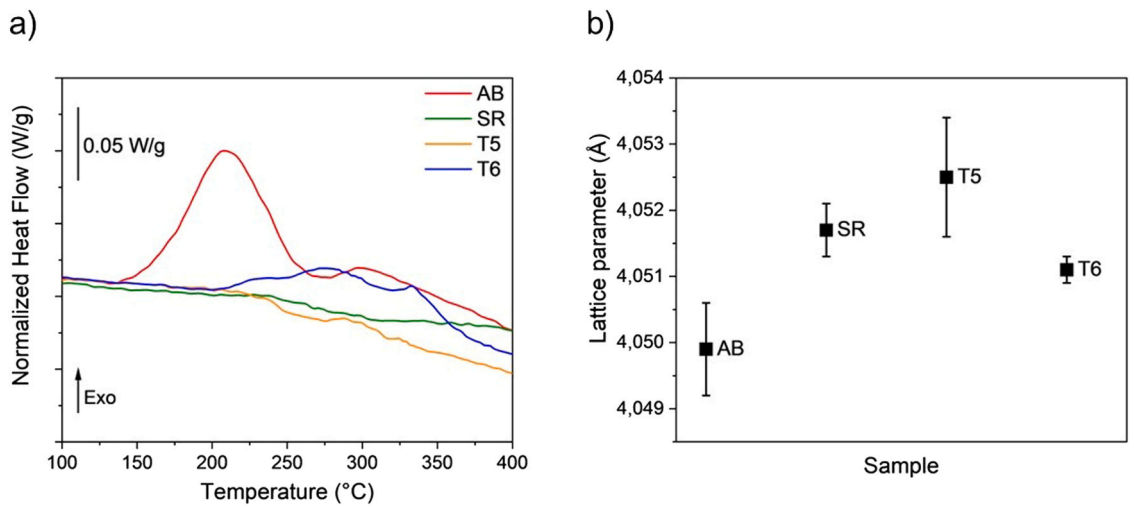

Fig. 4. DSC curves related to the precipitation of Si and other impurities present in the alloy from the Al matrix (a). Changes of Al lattice parameter upon different tempers (b).

These results were confirmed using the cosθcotθ method to determine the Al lattice parameter starting from the XRD patterns (Fig. 4b). Since it is known in the literature that Si lowers the lattice parameter of Al [14, 15], it is possible to evaluate the amount of Si supersaturated in the Al matrix upon the different tempers. In particular, Si supersaturation was observed to follow the order AB > T6 > SR > T5, indicating the same hierarchic behavior coming from the DSC measurements. Both the DSC and XRD results confirm what was observed from the micrographs and agree to recognize the T5 and SR tempers as the most suitable to increase the electrical conductivity of the AlSi7Mg alloy.

The equivalent surface electrical resistivity results obtained on the WR75 and WR28 test cavities, operating respectively at 10 GHz and at 30 GHz, are reported in Table 1. Resistivity increases following the order T5 < SR < T6 < AB, which is the same hierarchy obtained using the previous techniques though confirming that the samples subjected to the T5 heat treatment are those possessing the best electrical conductivity for the intended application. It is interesting to underline that this result is reproduced for two test cavities tested at different operating frequencies, i.e 10 GHz and at 30 GHz. The scatter in the values reported in Table 1 is most likely related to other factors affecting the measurement, such as the dimensional accuracy and the surface roughness, which are beyond the scope of this work. (Table 2)

Overall, a simple characterization allowed us to evaluate the effect of three different thermal treatments on the electrical conductivity of the AlSi7Mg alloy. The eutectic Si morphology and the samples' supersaturation are efficient parameters to account for when designing the thermal treatment to be applied to a component, especially if the final goal is to improve the electrical conductivity. Since both Si supersaturation and electrical conductivity decrease following the order AB > T6 > SR > T5; the T5 and SR tempers were indicated as the most suited to be applied when good electrical conductivity is the principal requirement for the final application. Microhardness tests were performed to verify which temper leads to the higher mechanical properties. The results showed a consistent hardness difference; the sample heat treated with the T5 temper is harder (122 ± 1 HV) than the one subjected to the SR treatment (84 ± 1 HV). For these reasons, the T5 temper can be identified as the best heat treatment to be applied to the AlSi7Mg alloy.

Table 2
Equivalent surface electrical conductivity measured on the WR75 and on the WR28 test cavities subjected to different tempers.

Thermal treatment	WR75 Equivalent surface electrical resistivity [μΩcm]	WR28 Equivalent surface electrical resistivity [μΩcm]
AB	21	50
SR	17	25
T5	14	15
T6	18	32

4. Conclusions

From the microstructural and structural characterization of both cubic samples and waveguide test cavities in AlSi7Mg alloy by PBF-LB/M it is possible to state that:

- The analysis of the eutectic Si morphology suggests that samples subjected to the T5 and to the SR heat treatments possess the highest electrical conductivity.
- DSC and XRD analysis confirmed that the T5 and the SR thermal treatments can promote the complete Si precipitation from the supersaturated Al matrix resulting from the rapid cooling rates typical of the PBF-LB/M process. This finding suggests that these treatments are the most promising for AlSi7Mg alloy in applications requiring good electrical conductivity.
- The equivalent surface electrical resistivity increases following the order T5 < SR < T6 < AB.
- The samples subjected to the T5 heat treatment result in the best electrical conductivity and hardness, making this temper the preferred choice for the production of waveguide components operating at different frequencies.

CRediT authorship contribution statement

Flaviana Calignano: Writing – review & editing, Validation. **Diego Manfredi:** Writing – review & editing, Supervision, Funding acquisition, Conceptualization. **Giuseppe Addamo:** Validation, Software. **Oscar Antonio Peverini:** Writing – review & editing, Validation, Supervision. **Mauro Lumia:** Validation, Investigation. **Silvia Marola:** Writing – original draft, Validation, Methodology, Conceptualization.

Declaration of Competing Interest

The authors declare that they have no known competing financial interests or personal relationships that could have appeared to influence the work reported in this paper.

Data availability

Data will be made available on request.

Acknowledgements

This work has been carried out under the GSTP General Support Technology Programme activity 18.1ET.03 of the European Space Agency, implemented through the contract 4000127300/19/NL/HK. The authors acknowledge Thales Alenia Space Italia, prime contractor, and Beam-IT SpA, project partner, for the fruitful collaboration provided in the context of the aforementioned programme. The view expressed herein can in no way be taken to reflect the official opinion of the European Space Agency.

References

[1] O.A. Peverini, M. Lumia, G. Addamo, G. Virone, N.J.G. Fonseca, How 3D-printing is changing RF front-end design for space applications, IEEE J. Microw. 3 (2) (2023) 800–814.
[2] M. Kilian, C. Hartwanger, M. Schneider, M. Hatzenbichler, Waveguide components for space applications manufactured by additive manufacturing technology, IET Microw. Antennas Propag. 11 (14) (2017) 1949–1954.
[3] F. Calignano, O.A. Peverini, G. Addamo, F. Paonessa, D. Manfredi, M. Galati, A. Salmi, E. Atzeni, P. Minetola, L. Iuliano, High-performance microwave waveguide devices produced by laser powder bed fusion process, Procedia CIRP 79 (2019) 85–88.
[4] X. Cui, H. Cui, Y. Wu, X. Liu, The improvement of electrical conductivity of hypoeutectic Al-Si alloys achieved by composite melt treatment, J. Alloy. Compd. 788 (2019) 1322–1328.
[5] L.F. Gomes, P.S. da Silva, A. Garcia, J.E. Spinelli, Effects of silver content and cooling rate on electrical conductivity and tensile properties of Al-Si(-Ag) Alloys, J. Mater. Eng. Perform. 29 (10) (2020) 6849–6860.
[6] H. Ye, X. Cui, X. Li, H. Cui, B. Zhang, H. Li, Y. Pan, R. Feng, Y. Wu, X. Liu, Fabrication of hypoeutectic Al-4Si alloy with high electrical conductivity, high plasticity and medium strength by the dual treatment of Al matrix and eutectic Si microstructure, J. Alloy. Compd. 885 (2021), 161117-161117.
[7] J.Q. Gan, Y.J. Huang, C. Wen, J. Du, Effect of Sr modification on microstructure and thermal conductivity of hypoeutectic Al−Si alloys, Trans. Nonferrous Met. Soc. China 30 (2020) 2879–2890.
[8] S. Marola, D. Manfredi, G. Fiore, M.G. Poletti, M. Lombardi, P. Fino, L. Battezzati, A comparison of selective laser melting with bulk rapid solidification of AlSi10Mg alloy, J. Alloy. Compd. 742 (2018).
[9] P. Van Cauwenbergh, V. Samaee, L. Thijs, J. Nejezchlebová, P. Sedlák, A. Iveković, D. Schryvers, B. Van Hooreweder, K. Vanmeensel, Unravelling the multi-scale structure–property relationship of laser powder bed fusion processed and heat-treated AlSi10Mg, Sci. Rep. 11 (1) (2021).
[10] P. Uliasz, T. Knych, M. Piwowarska, J. Wiecheć, The Influence of Heat Treatment Parameters on the Electrical Conductivity of AlSi7Mg and AlSi10Mg Aluminum Cast Alloys, IN: H. Weiland, A.D. Rollett, W.A. Cassada (Eds.) 13th International Conference on Aluminum Alloys (ICAA13), TMS (The Minerals, Metals & Materials Society), 2012, pp. 129-135.
[11] F. Calignano, V. Mercurio, G. Rizza, M. Galati, Investigation of surface shot blasting of AlSi10Mg and Ti6Al4V components produced by powder bed fusion technologies, Precis. Eng. 78 (2022) 79–89.
[12] F. Heringhaus, H.J. Schneider-Muntau, G. Gottstein, Analytical modeling of the electrical conductivity of metal matrix composites: application to Ag-Cu and Cu-Nb, Mater. Sci. Eng. A 347 (1-2) (2003) 9–20.
[13] L. Tian, I. Anderson, T. Riedemann, A. Russell, Modeling the electrical resistivity of deformation processed metal-metal composites, Acta Mater. 77 (2014) 151–161.
[14] W.B. Pearson, A Handbook of Lattice Spacings and Structures of Metals and Alloys, Pergamon Press, 1967.
[15] S. Steeb, H. Warlimont, Rapidly quenched metals, in: S. Steeb, H. Warlimont (Eds.), Proceedings of the Fifth International Conference on Rapidly Quenched Metals, North-Holland Physics Publishing, Wurzburg, Germany, 1984.